

Quantitative I-131 SPECT Reconstruction using CT Side Information from Hybrid Imaging

Yuni K. Dewaraja, *Member, IEEE*, Kenneth F. Koral, and Jeffrey A. Fessler, *Fellow, IEEE*

Abstract— A penalized-likelihood (PL) SPECT reconstruction method using a modified regularizer that accounts for anatomical boundary side information was implemented to achieve accurate estimates of both the total target activity and the activity distribution within targets. In both simulations and experimental I-131 phantom studies, reconstructions from 1) penalized likelihood employing CT-side information based regularization (PL-CT); 2) penalized likelihood with edge preserving regularization (no CT); 3) penalized likelihood with conventional spatially invariant quadratic regularization (no CT) were compared with 4) Ordered Subset Expectation Maximization (OSEM), which is the iterative algorithm conventionally used in clinics for quantitative SPECT. Evaluations included phantom studies with perfect and imperfect (misregistered) side information and studies with uniform and non-uniform activity distributions in the target. For targets with uniform activity, the PL-CT images and profiles were closest to the ‘truth’, avoided the edge offshoots evident with OSEM and minimized the blurring across boundaries evident with regularization without CT information. Apart from visual comparison, reconstruction accuracy was evaluated using the bias and standard deviation (STD) of the total target activity estimate and the root mean square error (RMSE) of the activity distribution within the target. PL-CT reconstruction reduced both bias and RMSE compared with regularization without side information. When compared with unregularized OSEM, PL-CT reduced RMSE and STD while bias was comparable. For targets with non-uniform activity, these improvements with PL-CT were observed only when the change in activity was matched by a change in the anatomical image and the corresponding inner boundary was also used to control the regularization. In summary, the present work demonstrates the potential of using CT side information to obtain improved estimates of the activity distribution in targets without sacrificing the accuracy of total target activity estimation.

I. INTRODUCTION

There is much interest in accurate quantitative single photon emission computed tomography (SPECT) imaging for dosimetry in internal emitter therapies such as I-131 radioimmunotherapy (RIT) and radioiodine therapy. It has been hypothesized that the efficacy of such therapies is determined not primarily by the mean radiation absorbed dose to the tumor, but rather by other measures that represent the 3D distribution of absorbed dose. Hence in recent dose-

response studies, in addition to the mean dose, there has been much interest in evaluating other summary measures including the dose volume histogram and the equivalent uniform dose. For such evaluations it is important to achieve accurate estimates of both the total target activity and the activity distribution within the target.

Currently, the conventional iterative reconstruction algorithm for SPECT is unregularized 3D Ordered-Subset Expectation Maximization (OSEM), often followed by post-reconstruction filtering to reduce image noise. Indiscriminate smoothing including across region boundaries degrades recovery of activity. Using 3D OSEM with no post-reconstruction filtering, good quantification accuracy can be achieved when a large number of iterations are used, but at the expense of significant edge artifacts and considerable noise [1][2]. In previous I-131 studies our group has achieved reasonably good target activity quantification accuracy with 3D OSEM, [3][4], but problems with edge artifacts and the accuracy of the activity distribution were not addressed. In the present study, to achieve accurate estimates of both target activity and the activity distribution within the target, a penalized-likelihood approach to SPECT reconstruction using a modified regularizer that accounts for anatomical (CT) boundary information is implemented and evaluated. The side information controls the regularization by allowing smoothing in uniform regions, but preventing the smoothing across region boundaries to avoid activity spillover between distinct regions.

In positron emission tomography (PET), reconstruction accuracy has been improved by using anatomical side information during the emission tomography reconstruction [5][6][7]. In SPECT, most studies have investigated using anatomical boundary information in a post-reconstruction step [8][9][10] or using joint estimation [11][12]. Unlike the intra-reconstruction approach of the present study, the post-processing approach requires an assumption of uniform uptake within the target. Although joint estimation can potentially compensate for large alignment error it is computationally intensive and currently not suitable for clinical processing of 3D data. For hybrid imaging systems where SPECT-CT misregistration is minimized, we investigate the simpler method where anatomical boundary information is used during the penalized-likelihood reconstruction.

II. METHODS

A. Measurement Model and Iterative Algorithm

We used the standard Poisson statistical model for emission tomography, where each raw measured SPECT projection value has a mean that is related linearly to the unknown

Manuscript received November 13, 2009. This work was supported in part by grant 2R01 EB001994 awarded by the National Institutes of Health, United States Department of Health and Human Services.

Y.K. Dewaraja and K.F. Koral are with the Department of Radiology, University of Michigan, Ann Arbor, MI 48109, USA (e-mail: yuni@umich.edu).

J.A. Fessler is with the Department of Electrical Engineering and Computer Science, University of Michigan, Ann Arbor, MI 48109, USA.

voxelized activity distribution via one row of a system matrix. For the forward and backprojector we used the rotate-sum method [13] using bilinear interpolation for rotating the current estimate of the activity distribution and the attenuation map. The SPECT camera evaluated here uses a contouring orbit so the depth-dependent detector/collimator response was adjusted for each projection view based on the corresponding distance of the collimator to the isocenter. Our implementation uses a backprojector that is exactly matched to the transpose (adjoint) of the forward projector. A triple energy window based scatter estimate was included in the statistical model as a known additive term as appropriate for Poisson statistics. We have previously implemented 3D OSEM with this system model [3]. For the regularized case, we used an ordered-subsets iterative algorithm based on a paraboloidal surrogates method [14] [15]. Software for these methods is available [16].

B. Regularizing Penalty Function

For simplicity we describe the regularizers in 1D; the extension to 3D is straightforward but notationally cumbersome. In 1D the conventional quadratic regularizer [17] for an object with N voxels with values f_j is

$$R(f) = \beta \sum_{j=2}^N (f_j - f_{j-1})^2$$

where the regularization or smoothness parameter β controls the strength of the regularization. This regularizer will control noise but also blurs the activity across image boundaries between different regions. To reduce this blur, we also investigated edge-preserving regularization using the convex, nonquadratic, Huber function [18].

Neither of the preceding regularizers use any anatomical side information. To incorporate side information, we modify the quadratic regularizer as follows:

$$R(f) = \beta \sum_{j=2}^N w_j (f_j - f_{j-1})^2$$

where the regularization weights w_j control the strength of regularization between neighboring voxel values f_j and f_{j-1} . Ideally we would like $w_j = 1$ within uniform regions and $w_j = 0$ when voxels j and $j-1$ correspond to regions with different activity levels, to avoid blur between those distinct regions [5].

In practice there are not distinct boundaries between different regions because of the finite voxel size, particularly in SPECT. Suppose the CT image is segmented into K different regions, and let l_{jk} denote the “labels” that indicate whether voxel j belongs to region k . Ideally these region masks would be binary, with each voxel belonging to one and only one region. In our application however, tumors are outlined on CT space (typically 512×512) and must be re-sampled to SPECT space (typically 128×128). Due to the finite size of the SPECT voxels relative to the CT voxels, our region masks take values in the interval $[0, 1]$, with $\sum_{k=1}^K l_{jk} = 1$. In the interior of a region the values of l_{jk} are 0 or 1, but there are intermediate values around the boundaries of

each region. The presence of these intermediate values leads to an open question of how to choose the corresponding regularization weights w_j . We used the following approach.

First we formed a “label” image $l_j = \sum_{k=1}^K k l_{jk}$. Most voxels in

this label image take discrete values in the set $\{1, 2, \dots, K\}$ but there are intermediate values near region boundaries. Then we defined the regularization weights using thresholded differences of the label image (we chose the threshold $\epsilon=0.1$).

$$w_j = \begin{cases} 1, & |l_j - l_{j-1}| \leq \epsilon \\ 0, & \text{otherwise} \end{cases}$$

We also investigated the ‘blurred label’ method [6] for defining the regularization weights to account for the uncertainty associated with mismatched anatomical information. We found that ‘blurred labels’ did not work as well as the above approach for the non-binary region masks of the present application. Optimizing regularization weights w_j for non-binary masks remains an open problem for future work.

The regularization parameter β was chosen to obtain a desired resolution of the reconstructed image as previously proposed [19]. When β is too small the reconstructed image will be very noisy, while if β is too large the image will be very smooth, hence resulting in a loss of useful information. We took the practical approach of choosing β by looking at the point spread function (away from region boundaries) to get a target FWHM of ~ 1 cm (2 pixels).

The OSEM reconstruction was used as the initial estimate for the regularized reconstructions. Considering convergence, noise, the edge artifacts and the computation time we choose to use 40 OSEM iterations (6 subsets) for the initial estimate followed by 30 iterations with the regularized algorithm. The computation time with either algorithm was about 200 sec for 10 iterations on a 3 GHz dual processor Mac Pro.

C. Phantom Studies

Both simulated and experimental I-131 phantom studies were performed to evaluate the reconstructions. The camera modeled/used was a Siemens Symbia TruePoint SPECT/CT with a high-energy parallel-hole collimator, and the following acquisition parameters for the experimental measurements: 180° and 30 stops per head; body contouring; 20% photopeak at 364 keV; two adjacent 6% scatter correction windows; and a 128×128 matrix with a pixel size of 4.8 mm. The CT data were reconstructed with a $512 \times 512 \times 196$ matrix and 0.98 mm x 0.98 mm x 2 mm voxel size.

Simulations

Targets with uniform activity: The simulated phantom geometry consisted of six (95 ml, 61 ml, 17 ml, 11 ml, 8 ml and 4 ml) hot spheres in a warm elliptical tank of dimensions 23 cm x 32 cm x 21 cm (Fig. 1). Activity within the spheres was uniformly distributed and all spheres had the same contrast; the sphere to background activity concentration ratio

was 6:1. Projections were scaled to 50 million total counts before the addition of Poisson distributed noise to obtain 10 noisy realizations. This represents a typical noise level for patient imaging in I-131 RIT.

The true boundaries of the simulated object were used when defining the label image. The label image was non-binary with intermediate values near boundaries as will be the case with clinical data. Simulation studies were performed for two conditions 1) with accurate alignment of the SPECT data and the target boundaries, representing perfect side information and 2) with the SPECT data translated by 5 mm with respect to the target boundaries, mimicking imperfect side information due SPECT-CT misregistration.

Targets with non-uniform activity: In patient imaging the activity distribution within tumors can be non-uniform. Hence, the activities of the 3 largest spheres of the previous simulation were changed to add some degree of non-uniformity within the target. The modified spheres had an inner core and an outer shell, with an activity concentration ratio of 6:4:1 for core to shell to background (Fig 2).

The labels image for the non-uniform targets were defined in two ways 1) using boundaries of both the inner core and the outer shell and 2) using only the outer boundary of the target. The first represents the case where the non-uniformity in the target uptake visible on SPECT is matched by a corresponding anatomical change visible on CT. The second case represents the situation where there is a mismatch between the inhomogeneity seen on SPECT and that visible on CT.

Experimental Measurements

Two spherical shells (Data Spectrum, Inc) with an inner core and an outer shell fillable with different activity concentrations were positioned on either side of a center sphere (95 mL) in the elliptical tank (Fig 3). The center sphere to background activity concentration ratio was 4:1. In the larger spherical shell, the inner core (31 mL) was left ‘cold’ (representing a tumor with a necrotic center) while the outer shell (84 mL) was filled with I-131 to get an outer shell to background activity concentration ratio of 3:1. In the smaller spherical shell the inner core was 5.5 mL while the outer shell was 21 mL and the core to shell to background activity concentration ratio was 13:4:1. Multiple (eight) 30 min sequential acquisitions were performed under identical conditions.

Target boundaries were drawn in CT space and were re-sampled to SPECT space to define the label image 1) using both inner core and outer shell boundaries and 2) using only the outer boundary of the target.

III. RESULTS

For both simulated and measured phantom data, we compared reconstructions from 1) unregularized OSEM with no post-filtering; 2) penalized likelihood employing CT-side information based regularization (PL-CT); 3) penalized likelihood with edge preserving regularization (PL-EP) (no CT); 4) penalized likelihood with conventional spatially invariant quadratic regularization (PL-Q) (no CT). In addition to visual comparison of images and profiles quantitative

evaluation of the different SPECT reconstructions were carried out for each target based on the mean estimated bias, STD and RMSE in counts (simulation) or activity (experiments). In the case of experimental measurement, the conversion from SPECT counts to activity was carried out using the camera calibration factor (counts per sec per MBq) determined from experimental measurement with a known amount of activity distributed in an elliptical phantom. The bias is a measure of how close the SPECT estimated total target counts (or activity) is to the true total target counts (or activity), while the RMSE as defined below is a measure of how close the count (or activity) distribution within the target is to the true target count (or activity) distribution. The VOI for the target was the true object in the case of simulation and the CT-defined object in the case of experimental measurement. In addition, evaluations were also performed for VOIs with a radius 5 mm larger than the object radius. The RMSE of object i with voxels n_i was defined as:

$$RMSE_i = \sqrt{\frac{1}{N} \frac{1}{n_i} \sum_{j=1}^N \sum_{k=1}^{n_i} (x_{j,k} - t_k)^2}$$

where N is the number of realizations, $x_{j,k}$ is the estimated counts (or activity) value of voxel k for realization j and t_k is the true value.

A. Simulation studies

Targets with uniform activity: Fig 1 compares different reconstructions of a single noisy realization of the phantom with uniform activity targets. Visually, the PL-CT reconstruction is closer to the true image than the other reconstructions. As evident from the images and profiles, unregularized OSEM with no post-filtering is noisy and produces significant edge overshoots, which result in a ‘cavity’ at the center of the larger spheres. This artifact is not evident in the PL-CT reconstruction. The images and profiles corresponding to regularization without side information are less noisy, but there is considerable blurring across boundaries, which is minimized with PL-CT.

The %bias, %STD and %RMSE in SPECT counts with the different reconstructions are compared in Table 1 for the case where there is no SPECT-CT misalignment and in Table 2 for the case where the SPECT and CT data is misaligned by 5 mm. For all the targets, the PL-CT reconstruction is superior to OSEM in terms of RMSE and STD, and is superior to the regularization without side information in terms of RMSE and bias. The bias with PL-CT is almost the same as with unregularized OSEM for the larger spheres, but is slightly worse for the two smallest spheres. The spatially invariant regularization results in the lowest STD.

The results given in Tables 1 and 2 were calculated for a VOI corresponding to the physical size of the object. When a VOI with a radius 5 mm larger than the true size was used the bias, STD and RMSE results followed the same trends shown in these tables. However with the larger VOI bias values for the smaller spheres were significantly better.

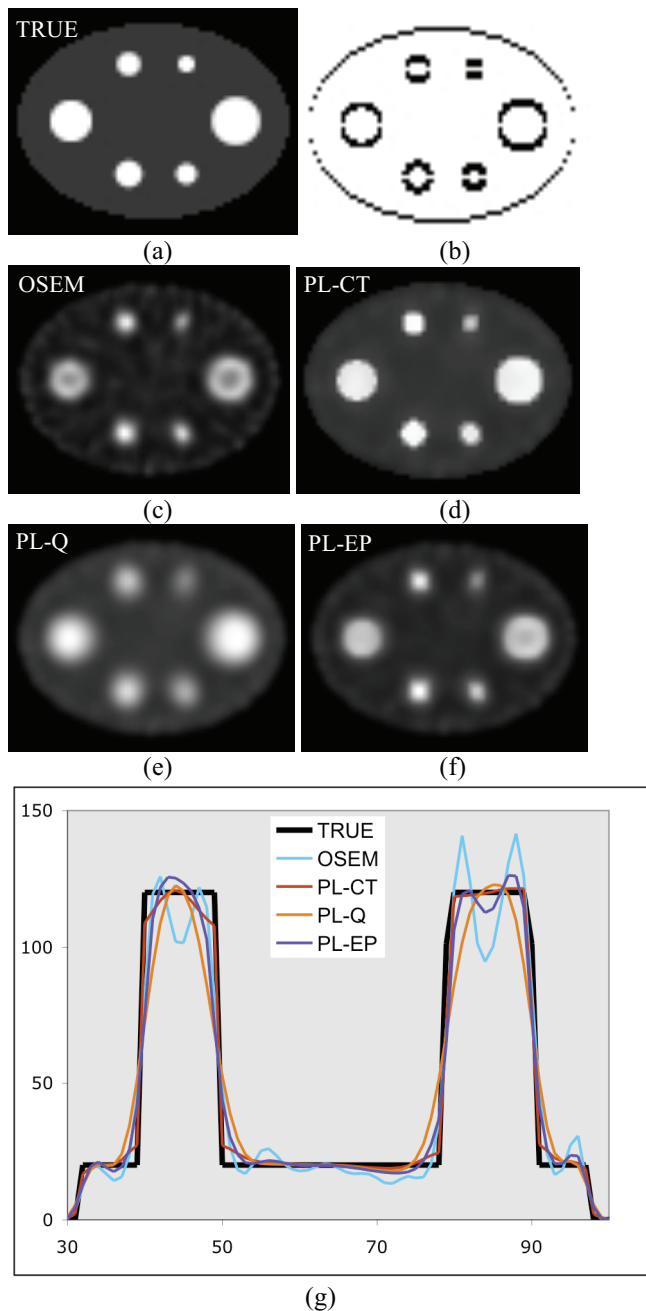


Fig 1: Images and profiles for a single realization of the simulation with uniform activity spheres. (a) True activity (b) regularization weights for PL-CT (c) OSEM (d) PL-CT (e) PL-Q (f) PL-EP and (g) profiles across center of image.

Targets with non-uniform activity: Fig 2 compares images and profiles of a single noisy realization of the phantom with non-uniform activity targets. The OSEM reconstruction is compared with the two PL-CT reconstructions (with and without using the inner boundaries when determining regularization weights). Although the OSEM reconstruction is still noisy, the significant edge artifacts evident in the case of uniform activity targets are greatly reduced here (the ‘cavity’ evident in the OSEM reconstruction of Fig 1 is not evident in Fig 2). The PL-CT reconstruction using both inner and outer boundaries (Fig 2 (c)) is closer to the true activity distribution

than both OSEM and the PL-CT reconstruction using only the outer boundary. When the inner boundary is not used to control the regularization there will be blurring across this boundary leading to loss of useful information as evident in Fig 2(d) and the corresponding profile.

The results shown in Table 3 follow the same trends seen for the uniform activity targets (PL-CT consistently gives better RMSE values). There was no significant difference in the bias and STD for PL-CT with and without using the inner boundaries because these measures use the total counts within the target defined by the outer boundary. However, when the inner boundary is not used to control the regularization the RMSE, which is a measure of the inaccuracy of the count distribution, increases due to the blurring across the inner boundary. In this case, the RMSE for PL-CT (given in parenthesis) is no longer superior to OSEM or the regularization without side information

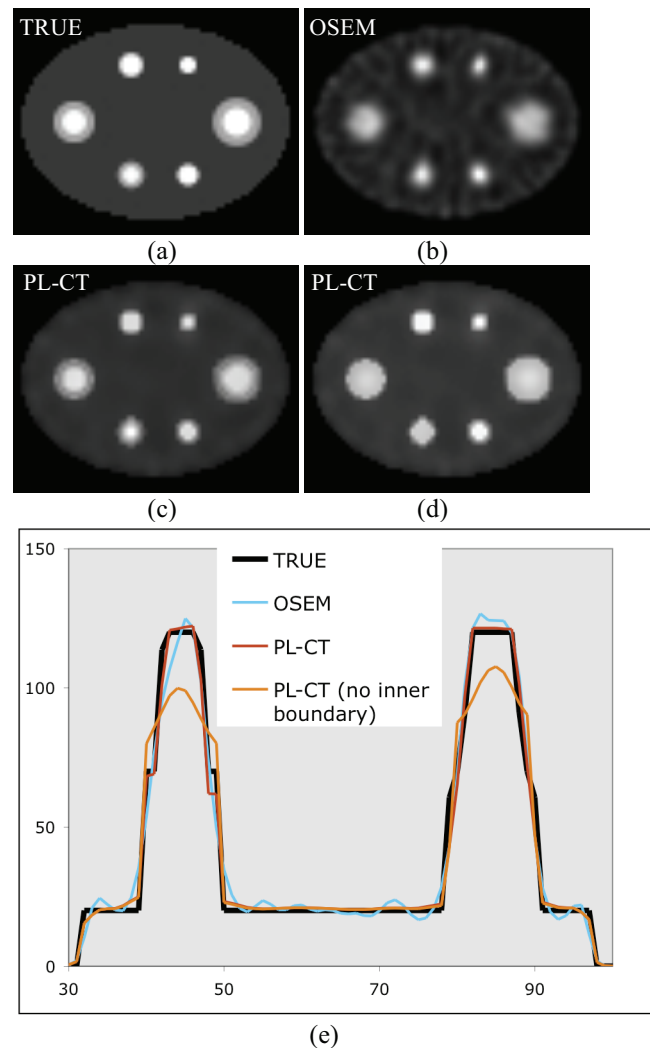


Fig 2: Images and profiles for a single noisy realization of the simulation with non-uniform activity spheres. (a) True activity (b) OSEM (c) PL-CT with inner and outer boundary (d) PL-CT with only outer boundary and (e) profiles across center of image.

Table 1: %Bias, %STD and %RMSE in VOI counts for the simulation of uniform activity spheres (with perfect SPECT-CT registration) (Fig 1).

Sphere (mL)	OSEM			PL-CT			PL-Q			PL-EP		
	Bias	STD	RMSE	Bias	STD	RMSE	Bias	STD	RMSE	Bias	STD	RMSE
95	5	0.2	17	5	0.2	13	19	0.1	23	9	0.2	17
61	6	0.4	18	6	0.3	14	23	0.2	26	11	0.3	19
17	12	1.4	25	12	1.2	19	37	0.9	34	20	1.4	27
11	11	1.3	23	12	1.1	18	39	0.6	36	20	1.2	26
8	14	1.9	23	16	1.8	21	45	1.4	39	26	2.0	26
4	24	3.4	26	28	2.8	27	54	1.7	47	39	3.3	36

Table 2: %Bias, %STD and %RMSE in VOI counts for the simulation of uniform activity spheres (with SPECT-CT mis-registration of 5 mm).

Sphere (mL)	OSEM			PL-CT			PL-Q			PL-EP		
	Bias	STD	RMSE	Bias	STD	RMSE	Bias	STD	RMSE	Bias	STD	RMSE
95	8	0.3	24	8	0.3	19	21	0.2	26	12	0.3	23
61	10	0.2	26	9	0.2	21	24	0.1	28	14	0.2	26
17	17	0.9	33	17	0.8	26	39	0.6	37	24	0.8	34
11	18	0.9	34	18	0.8	27	42	0.5	39	26	0.9	35
8	21	1.3	34	23	1.2	29	47	0.8	41	31	1.2	35
4	32	2.2	38	35	2.1	36	56	1.4	49	44	2.4	42

Table 3: %Bias, %STD and %RMSE in VOI counts for the simulation of non-uniform activity spheres (Fig 2). The values in parenthesis for PL-CT correspond to the case where the inner boundary was not used to control the regularization.

Sphere (mL)	OSEM			PL-CT			PL-Q			PL-EP		
	Bias	STD	RMSE	Bias	STD	RMSE	Bias	STD	RMSE	Bias	STD	RMSE
95	4	0.3	15	3	0.3	12 (17)	14	0.2	17	8	0.3	15
61	5	0.4	15	4	0.4	12 (18)	17	0.3	20	10	0.4	15
17	7	0.9	15	8	0.7	14 (18)	31	0.4	31	17	0.8	19

B. Experimental studies

Targets with non-uniform activity: Images and profiles from the experimental phantom study, which included non-uniform activity spheres are compared in Fig 3. Fig 3(a) is the CT image used to define the sphere boundaries including the boundaries of the inner core. The outlines were then resampled to SPECT space to determine the weights for the PL-CT regularization. The true activity distribution in SPECT space is given in Fig 3(b) followed by the different SPECT reconstructions in Fig 3 (c)-(f). The images and profiles show that in general the activity distribution from PL-CT (using both inner and outer boundaries) is closer to the true distribution than OSEM and the regularizations without CT information. In the cold region however, the profile for unregularized OSEM is closer to the truth.

Table 4 compares %bias, %STD and %RMSE for the uniform center sphere and the two non-uniform spherical shells. PL-CT (using both the inner and outer boundaries) is superior to OSEM in terms of RMSE and STD while the bias is comparable. As in the simulation, when the inner core boundary information is not used in the PL-CT reconstruction, the bias and STD is not significantly affected, but the RMSE (given in parenthesis) increases due to blurring across this boundary.

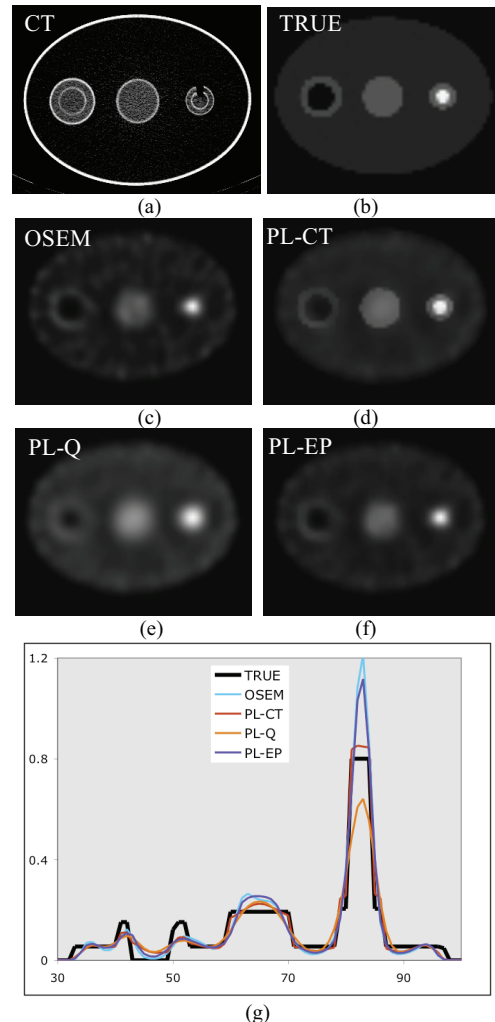


Fig 3: Images and profiles for phantom measurement. (a) CT (b) True activity (c) OSEM (d) PL-CT (e) PL-Q (f) PL-EP and (g) profiles across center.

Table 4: %Bias, %STD and %RMSE in SPECT measured activity for the experimental phantom with two non-uniform activity spheres (Fig 3). The value in parenthesis for PL-CT corresponds to the case where the inner core boundary was not used to control the regularization.

	OSEM			PL-CT			PL-Q			PL-EP		
	Bias	STD	RMSE	Bias	STD	RMSE	Bias	STD	RMSE	Bias	STD	RMSE
Uniform sphere	2	0.8	42	1	0.8	26	12	0.7	31	5	0.7	40
Sphere with hot core	-2	0.8	39	-3	0.7	18 (49)	13	0.7	42	0	0.7	35
Sphere with necrotic core	14	1.4	42	15	1.4	41 (49)	22	1.3	53	18	1.4	47

C. Clinical Application

To demonstrate clinical application, the penalized-likelihood reconstruction with CT-side information based regularization was applied to SPECT/CT imaging data from a patient imaged at our clinic 2 days after a 2.8 GBq (76 mCi) administration of I-131 tositumomab therapy for non-Hodgkin's lymphoma (NHL). In NHL, typically the tumors are well defined on CT and are relatively large [20]. Previously as part of an ongoing research study, SPECT data had been reconstructed with 3D OSEM and tumors in inguinal region had been defined on 512 x 512 CT to determine mean tumor absorbed dose. For the present work, the CT defined tumor outlines were resampled to SPECT space to determine the weights for the PL-CT regularization. A slice of the PL-CT reconstruction superimposed on CT is shown in Fig 4. The profile (across center of tumors) compares the PL-CT reconstruction with OSEM, PL-Q and PL-EP.

IV DISCUSSION AND CONCLUSION

Accurate determination of both target activity and activity distribution within the target is important for dosimetry-based treatment planning in internal emitter therapies such as I-131 radioimmunotherapy. A penalized likelihood reconstruction method employing CT side information based regularization was implemented and compared with regularization without side information and with unregularized OSEM. We chose to compare the PL reconstructions to OSEM with no post-filtering because currently we use this algorithm to quantify tumor activity for dosimetry studies [20].

In both simulation and experimental phantom studies with uniform activity targets the PL-CT reconstruction was clearly superior to OSEM and regularization without CT information (PL-Q and PL-EP) in terms of visual evaluation of images and profiles. The large distortions near the edges observed with OSEM become more severe as iterations proceed and have been observed previously in EM reconstructions of objects with sharp edges [1][2][21][22]. In the present study, PL-CT images and profiles did not display the significant edge overshoots evident with OSEM or the blurring across region boundaries evident in the methods where CT information was not used in the regularizer. Comparison of RMSE values also confirms that the PL-CT reconstruction resulted in the most accurate determination of target activity distribution. The improvement in estimation of activity distribution with PL-CT comes without sacrificing the accuracy of total target activity estimation as evident from the bias results. This is because the anatomical information was used to control the regularization, allowing smoothing within the target but avoiding smoothing

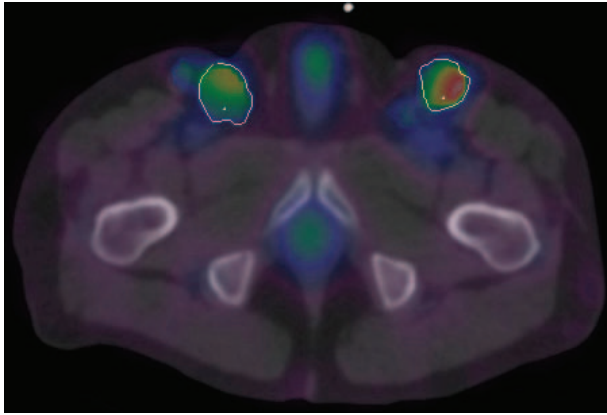
across boundaries. For quantification of total target activity, PL-CT was superior to regularization without side information and in general was comparable to unregularized OSEM. In both simulation and experimental measurement, the bias in activity estimate with PL-CT and OSEM was better than 17% for sphere sizes down to 17 mL but was up to 35% for the smallest 4 mL sphere. These relatively high bias values result from incomplete count recovery due to partial volume effects, which is particularly significant when imaging higher energy emitters such as I-131.

In simulation and experimental phantom studies with non-uniform activity targets, superior results with PL-CT were achieved only when the regularizer used anatomical boundary information that matched the activity non-uniformity. When the inner boundary was not used for regularization, the blur across this boundary resulted in the loss of useful information. In practice, the inner boundaries will not always be available since the non-uniformity may not be present in the anatomical image, or may not be visible on CT scans that are typically acquired with low-dose modes in hybrid systems. The improvements with PL-CT were achieved even with mis-registered side information (Table 2). The 5 mm translation simulated here is well within the capabilities of integrated SPECT-CT imaging. However, in patient imaging larger mis-alignment due to breathing is possible. Further investigation of methods to accommodate larger SPECT-CT misalignment in the PL-CT reconstruction is needed.

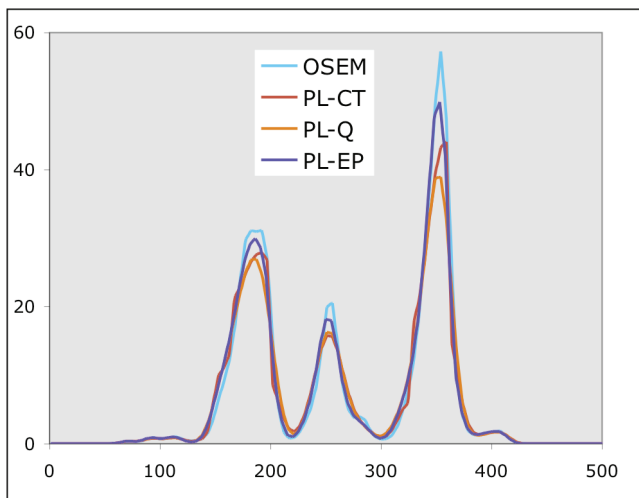
In summary, a penalized-likelihood SPECT reconstruction using a modified regularizer that accounts for CT-side information was implemented and compared to regularization without side information and to OSEM. Phantom evaluations demonstrated the potential of PL-CT to provide improved estimates of the activity distribution within targets and the total target activity when there is a good match between the SPECT and the CT information.

ACKNOWLEDGMENT

This work was supported by grant 2R01 EB001994 awarded by the National Institutes of Health, United States Department of Health and Human Services. The contents of the paper are solely the responsibility of the authors and do not necessarily represent the official views of the funding agency. The authors thank Dr Anca Avram and Dr Mark Kaminski for providing the data used in the patient example.



(a)



(b)

Fig 4 (a) patient PL-CT SPECT reconstruction superimposed on CT with tumor outline and (b) profiles across the tumor for the different reconstructions.

REFERENCES

- [1] Tsui BMW, Frey EC, Zhao X. The importance and implementation of accurate 3D compensation methods for quantitative SPECT. *Phys Med Biol* 1994;39:509-530.
- [2] Snyder DL, Miller MI, Thomas LJ, Politte DG. Noise and edge artifacts in maximum-likelihood reconstructions for emission tomography. *IEEE Trans Med Imag*, 6(3):228-238 September 1987.
- [3] Koral K, Yendiki A, Dewaraja YK. Recovery of total I-131 activity within focal volumes using SPECT and 3D OSEM. *Phys Med Biol* 52: 777-790, 2007.
- [4] Dewaraja YK, Wilderman SJ, Ljungberg M, Koral KF, Zasadny K, Kaminiski M. Accurate dosimetry in I-131 radionuclide therapy using patient specific, 3-dimensional methods for SPECT reconstruction and absorbed dose calculation. *J Nucl Med* 46:840-849, 2005.
- [5] Fessler JA, Clinthorne NH, Rogers WL. Regularized emission image reconstruction using imperfect side information. *IEEE Trans Nucl Sci* 1992;39:1464-1471.
- [6] Comtat C, Kinahan PE, Fessler JA et al. Clinically feasible reconstruction of 3D whole-body PET/CT data using blurred anatomical labels. *Phys Med Biol* 2002;47:1-20.
- [7] Nuyts J, Baete K, Beque D, Dupont P. Comparison between MAP and postprocessed ML for image reconstruction in emission tomography when anatomical knowledge is available. *IEEE Trans Med Imag*. 2005;24:667-675.

- [8] Boening G, Pretorius PH, King MA. Study of relative quantification of Tc-99 m with partial volume effect and spillover correction for SPECT oncology imaging. *IEEE Trans Nucl Sci* 2006;53:1205-1212.
- [9] Du Y, Tsui BMW, Frey EC. Partial volume effect compensation for quantitative brain SPECT imaging. *IEEE Trans Med Imag* 2005;24:969-975.
- [10] Dewaraja YK, Ljungberg M, Fessler JA. Anatomical information based partial volume compensation for I-131 SPECT imaging in radioimmunotherapy. *J Nucl Med* 2006;47:115P.
- [11] Bowsher JE, Johnson VE, Turkington TG et al. Bayesian reconstruction and use of anatomical A Priori information for emission tomography. *IEEE Trans Med Imaging* 1996;15:673-686.
- [12] Gindi G, Lee M, Rangarajan A, Zubal G. Bayesian reconstruction of functional images using anatomical information as priors. *IEEE Trans Med Imag* 12:670-80, 1993.
- [13] G. L. Zeng and G. T. Gullberg. Frequency domain implementation of the three-dimensional geometric point response correction in SPECT imaging. *IEEE Trans. Nuc. Sci.*, 39(5-1):1444-53, October 1992.
- [14] J. A. Fessler and H. Erdoĝan. A paraboloidal surrogates algorithm for convergent penalized likelihood emission image reconstruction. In Proc. IEEE Nuc. Sci. Symp. Med. Im. Conf., volume 2, pages 1132-5, 1998.
- [15] H. Erdoĝan and J. A. Fessler. Ordered subsets algorithms for transmission tomography. *Phys. Med. Biol.*, 44(11):2835-51, November 1999.
- [16] J. A. Fessler. Users guide for ASPIRE 3D image reconstruction software. Technical Report 310, Comm. and Sign. Proc. Lab., Dept. of EECS, Univ. of Michigan, Ann Arbor, MI, 48109-2122, July 1997. Available from <http://www.eecs.umich.edu/~fessler>
- [17] Fessler JA. Penalized weighted least squares image reconstruction for PET. *IEEE Trans Med Imag*. 13:290-300, 1994.
- [18] Huber PJ. *Robust Statistics*. New York: Wiley, 1981.
- [19] J. A. Fessler and W. L. Rogers. Spatial resolution properties of penalized-likelihood image reconstruction methods: Space-invariant tomographs. *IEEE Tr. Im. Proc.*, 5(9):1346-58, September 1996.
- [20] Dewaraja YK, Wilderman SJ, Koral KF, Kaminiski M, Avram AM. Use of Integrated SPECT/CT imaging for tumor dosimetry in I-131 radioimmunotherapy: a pilot patient study. *Cancer Biotherapy & Radiopharmaceuticals* 24: 417-426, 2009.
- [21] Koral KF, Kritzman JN, Rogers VE, Ackerman R, Fessler JA. Optimizing the number of equivalent iterations of 3D OSEM in SPECT reconstruction of I-131 focal activities. *Nucl Intr and Meth A*:579:326-329, 2007.
- [22] Shcherbinin S, Celler A. An investigation of accuracy of iterative reconstructions in quantitative SPECT. *J. Phys.:Conf. Ser.* 124 012044, 2008.